5 Towards a Fullerene Quantum Computer

To reach the final goal, a solid state quantum computer, a lot of technical problems have to be solved. Local addressing of the qubits is as necessary as the ability to change the interaction between the qubits. Last but not least, each single qubit has to be read out. In our case this means that single spin detection has to be possible. Groups throughout the world are working on different approaches (e.g., magnetic resonance force microscopy, STM, or optical detection) for single spin read–out. However, it will take some years to reach this milestone. So, to demonstrate the basic principles of the concept i. e., computing with electron spins using dipolar coupling, an easier way than the solid state concept has to be found.

Quantum computing without the necessity to switch the interaction between the qubits or to address them locally can be done with a Quantum Cellular Automaton (QCA) as proposed by Lloyd [65] or Benjamin [66]. Such a QCA consists of a chain built from three (Lloyd) or two (Benjamin) different types of qubits with a well defined interaction.

This chapter will show a route and first experimental results how to build such a chain from endohedral fullerenes, and how to provide a qubit interaction of a specific strength whilst avoiding the problem of single spin read–out.

5.1 A Fullerene–based Quantum Cellular Automaton

A QCA consists of a sequence of different qubits, e.g. A, B, and C, arranged on a string with couplings J_{AB}, J_{BC}, J_{CA} between them (Fig. 5.1 (a)). As a realisation of this automaton, the three endohedral fullerenes $^{14}N@C_{60}$, $^{15}N@C_{60}$, and $^{31}P@C_{60}$ can be used. With the chemical modification proposed by A. Hirsch [3,4] it is in principle possible to synthesise any sequence of the endohedral fullerenes (Fig. 5.1 (b)).

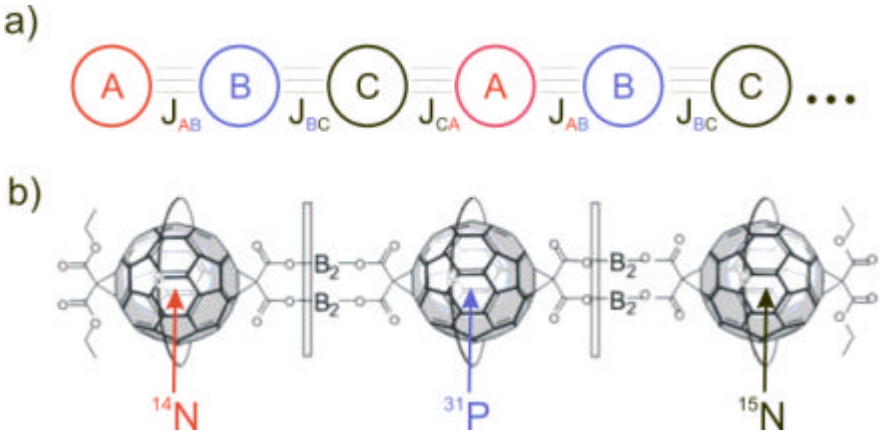

Fig. 5.1: (a) Schematic representation of an ABC – quantum cellular automaton. The different interactions J_{AB} etc. are indicated.

(b) Proposed realisation of this automaton by the three different endohedral fullerenes.

By changing the chemical intermediates between the fullerenes the distance can be varied. For the closest distance corresponding to touching fullerenes the maximum coupling between the endohedral spins is approximately 50 MHz (see chapter 2). The coherence time of e.g. $^{14}N@C_{60}$ is $T_2 \sim 20$ µs, fairly independent of temperature. Thus, the ratio of phase coherence to coupling time, $T_2/2J$, is up to 2000, allowing a sufficient number of operations.

A single cell of this QCA has been produced in co-operation with M. Speck at the Friedrich–Alexander University Erlangen–Nürnberg. Nitrogen has been implanted in C_{60} by ion–implantation forming $N@C_{60}$ diluted in C_{60}. Afterwards, $C_{51}H_{90}O_{12}$ cyclo–addends have been added. The resulting $N@C_{111}H_{84}O_{12}$ trans3,3,3-trisadduct is shown schematically Fig. 5.2 and will be referred to as N@Saturn.

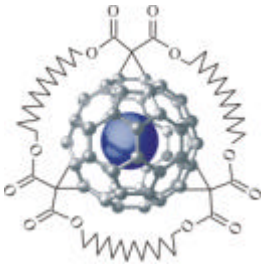

Fig. 5.2: The $C_{111}H_{84}O_{12}$ trans3,3,3–trisadduct with nitrogen inside. The endohedral fullerene was produced by ion–implantation before the cyclo–adduct has been added.

The ESR spectrum of a powder sample has been measured with a Miniscope MS100 (magnettech). The modulation amplitude was 0.02 mT, the modulation frequency 100 kHz, and the microwave power 3.5 mW. In Fig. 5.3, the data are shown after baseline correction and integration. The nitrogen triplet with the hyperfine constant a = 0.56 mT is clearly resolved and also a finestructure arising from zero–field splitting can be seen.

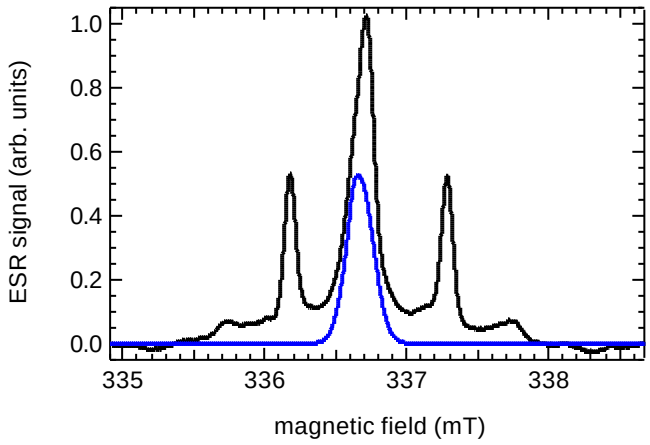

Fig. 5.3: The N@Saturn powder spectrum (black) clearly reveals the nitrogen hyperfine triplet and the finestructure arising from zero–field splitting. A peak (blue) known from impurities in half–filled dimers interferes with the data.

An additional line interferes with the centre line of the N@Saturn spectrum. This peak is known from the C_{60}–dimer arising from impurities, e.g. carbon dangling bonds [5], which are introduced by the chemical steps and which can be avoided if more effort is put into the subsequent purification as shown in chapter 5.3.

The zero–field splitting is known from various $N@C_{60}$ modifications and is due to deformation of the fullerene molecule [6-8]. It can be described as follows:

The part of the Hamiltonian that is responsible for the zero–field splitting or finestructure splitting is written as

$$H_{fs} = \mathbf{SDS} \tag{5.1}$$

with

$$\mathbf{D} = \begin{pmatrix} -\frac{1}{3}D + E & & \\ & -\frac{1}{3}D - E & \\ & & \frac{2}{3}D \end{pmatrix}. \tag{5.2}$$

Hence, D corresponds to the axial–symmetric deformation while E is the asymmetric part of the finestructure splitting.

If the magnetic field B_0 is applied in the direction of the z–axis of the axial–symmetric D tensor ($\vartheta = 0°$), the finestructure Hamiltonian reads as

$$\begin{aligned} H_{fs} &= -\frac{1}{3}S_x^2 D - \frac{1}{3}S_y^2 D + \frac{2}{3}S_z^2 D \\ &= S^2\left(-\frac{1}{3}D\right) + S_z^2 D \end{aligned} \tag{5.3}$$

with the expectation value of the state $|Sm_s\rangle$

$$\begin{aligned} &\langle Sm_s | S^2\left(-\frac{1}{3}D\right) + S_z^2 D | Sm_s \rangle \\ &= -S(S+1)\frac{1}{3}D + m_s^2 D \end{aligned} \tag{5.4}$$

Each energy level is shifted by a constant value. Additionally, there is a shift dependent on the state m_s. Therefore, the (±3/2, ±1/2) transitions are shifted with respect to the (1/2, -1/2) transition by $\pm[(3/2)^2\text{-}(1/2)^2]\cdot D = \pm 2D$ and the degeneracy is lifted. Each hyperfine line of the ESR spectrum splits into a finestructure triplet. The zero–field splitting depends on the angle ϑ as

$$\Delta B(J) = \mp\frac{D}{g_e m_B}(3\cos^2 J - 1). \tag{5.5}$$

The simulated position of the lines of one finestructure triplet is shown in the upper part of Fig. 5.4.

All angles ϑ are present in a powder sample. The intensity regarding to B_0 can be calculated by projecting the angle distribution onto the axis of the magnetic field weighted with the solid angle.

With equation (5.5), the intensity can be written as

$$I \propto \frac{d\Omega}{dB} = \sin J \frac{dJ}{dB} \approx \frac{1}{\cos J} = \sqrt{\frac{3}{\frac{B_0 - B}{D/g_e m_B} + 1}}. \qquad (5.6)$$

The simulation for the powder spectrum of one hyperfine line is shown in the lower part of Fig. 5.4.

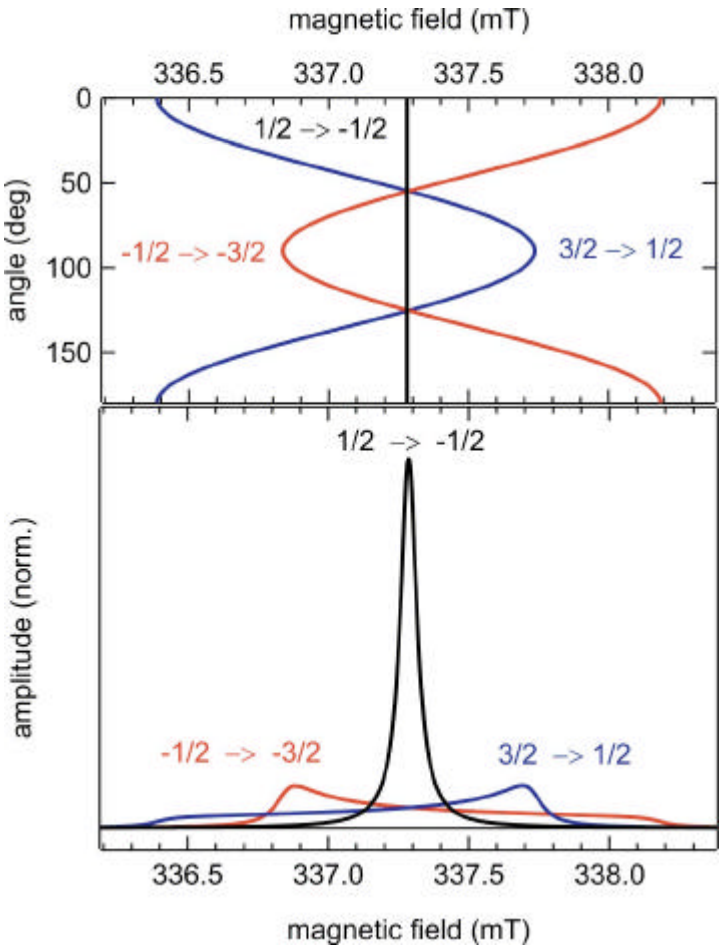

Fig. 5.4: Simulation of the field dependence of the three spin transitions, shown with field values corresponding to $m_I = 1$. The upper part shows the position of the finestructure lines for different angles J. In the lower part, the weighted projection of that dependence onto the magnetic field axis, is shown.

In Fig. 5.5, the interfering peak has been subtracted from the measured spectrum (black) and is compared to a nitrogen powder spectrum simulated with instrument parameters

taken from the measurement. An additional SDS finestructure has been assumed with an axial deformation $D/g_e\mu_B$ = 460 µT and a non–axial term $E/g_e\mu_B$ = 18 µT.

The values that describe the deformation of N@Saturn are a bit smaller than for the half–filled dimer with $D/g_e\mu_B$ = 480 µT and $E/g_e\mu_B$ = 30 µT [8] but much larger than the axial deformation for the malonic acid mono-adduct $N@C_{61}(COOC_2H_5)_2$ with $D/g_e\mu_B$ = 215 µT [7]. In the latter case, the non–axial deformation is nearly the same with $E/g_e\mu_B$ = 15 µT. The large axial deformation is due to the three addends forming a belt around the $N@C_{60}$, thus enlarging the diameter in one direction much more than a mono–adduct. Still, there is a non–axial term because the addends form a triangle and not a complete ring. If more of the N@Saturn molecules are strung together forming a chain, as needed for the quantum computing scheme, the axial term might be smaller. Such a behaviour has been found for the $N@C_{66}(COOC_2H_5)_{12}$ hexa–adduct [5].

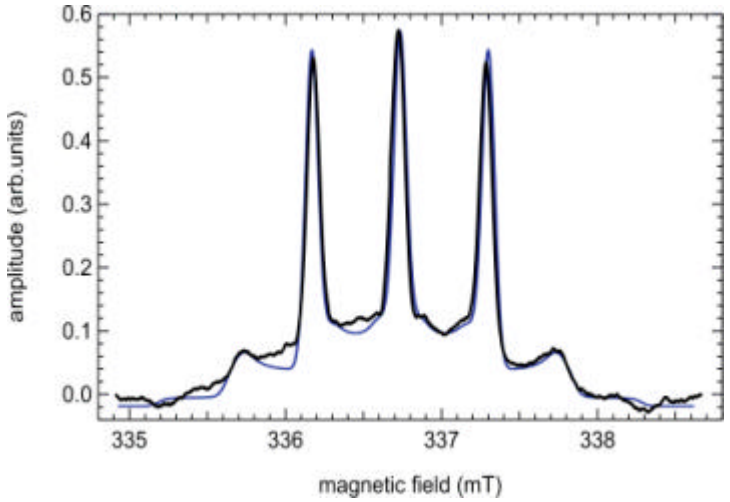

Fig. 5.5: The N@Saturn spectrum (black) without the impurity peak is compared to a simulated powder pattern (blue) using an axial deformation D = 460 µT and a non–axial term E = 18 µT.

For quantum computing with a spin system S = 3/2, all three spin transitions have to be accessible. Otherwise, it is impossible to implement the single qubit Hadamard gate for the subspace of one transition as discussed by J. Twamley [62]. Therefore, the presence of a zero–field splitting is beneficial as it splits the finestructure transitions.

However, in a powder sample, it will be not possible to address all finestructure transitions separately. As the zero–field splitting is angle dependent and all angles are present in a powder sample, there will always be a part of spins (individual qubits) with $D(\vartheta) = 0$. In this case, the spin subspaces mix, which is a source of strong decoherence.

A QCA requires a well defined alignment of the chain and, as we have to do ensemble computing, a lot of identical chains of identical orientation are needed. As long as the chains consist of only a few endohedral fullerenes, this can be done in principle by embedding them in a liquid–crystal matrix schematically shown for a $(N@C_{60})_2$ dimer in Fig. 5.6.

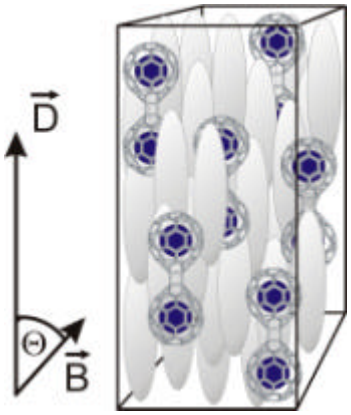

*Fig. 5.6: Schematic image of the embedding of fullerene dimers in a liquid crystal matrix. **D** indicates the average direction of the dimer molecules and **B** the external magnetic field.*

The zero–field splitting depends strongly on the angle T between the axis of the liquid crystal molecules and the applied magnetic field. This angle is given by the susceptibility χ of the liquid crystal and might be changeable by application of an electric field (as done in LC displays). The dipolar interaction between the endohedral spins will be tuned along with the line splitting as the angle dependency is the same.

This set–up would supply all requirements for a demonstration of the QCA scheme: ensemble read–out of qubit registers with a well defined coupling. The addressing of the qubits can be achieved by making use of the different resonance frequencies of nitrogen and phosphorous. If both qubits in a dimer are of the same type of endohedral fullerene, e.g. in a $(N@C_{60})_2$ dimer, the hyperfine splitting shifts the resonance frequencies of the qubits. In this case, only the sub–ensemble of molecules with different endohedral nuclear spins states m_I can be used for the computation.

The first step towards the orientation of a quantum register in a liquid crystal matrix is the alignment of endohedral monomers.

5.2 Alignment of $N@C_{60}$ and $N@C_{70}$ in a Liquid–Crystal Matrix

Non–spherical molecules can be geometrically aligned by embedding them in liquid crystals, which have a preferred orientation axis in an external field. Such an alignment of molecules can be extremely useful because elements of second–rank tensor interactions like dipolar coupling, nuclear quadruple interaction, or finestructure interaction can be determined with solution–like spectral resolution [10,11].

In the present experiment, as–prepared or slightly enriched (up to a concentration of $\sim 10^{-3}$ $N@C_{60}/C_{60}$) material was used. The fullerenes were dissolved at room temperature in the liquid crystal 4-Methoxybenzylidene-4'-n-butylaniline (MBBA) [12] in an ultrasonic bath. A surplus of fullerenes was added in order to obtain a saturated mixture which was then decanted, after the surplus fullerenes had sedimented at the bottom. In the nematic phase (between 293 K and 321 K for MBBA), the solute

molecules are directionally ordered due to the alignment of the elongated liquid crystal molecules in the external magnetic field (0.33 T).

A molecule with a non spherical symmetry will be aligned in turn with the liquid crystal molecules. The degeneracy of the finestructure transitions will be lifted due to the zero–field splitting as defined in equations (5.1)-(5.5). For liquid crystals, equation (5.5) is rewritten as

$$\Delta B(J) = 2\frac{D_{eff}}{g_e m_B} = 2\frac{D}{g_e m_B} O_{33} \tag{5.7}$$

with

$$O_{33} = \frac{1}{2}(3\overline{\cos^2\Theta} - 1), \tag{5.8}$$

where D describes the orientation of the molecules in the liquid crystal, and O_{33} is the order parameter of the uniaxial solute molecule in the liquid crystal. The average angle between the unique axis of the solute and the external magnetic field is described by Θ. In cases where the finestructure splitting is due to an induced deformation (see below), a clear separation into an intrinsic D and an orientation dependent O_{33} is not always possible, therefore mainly the product D_{eff} is used in the following discussion.

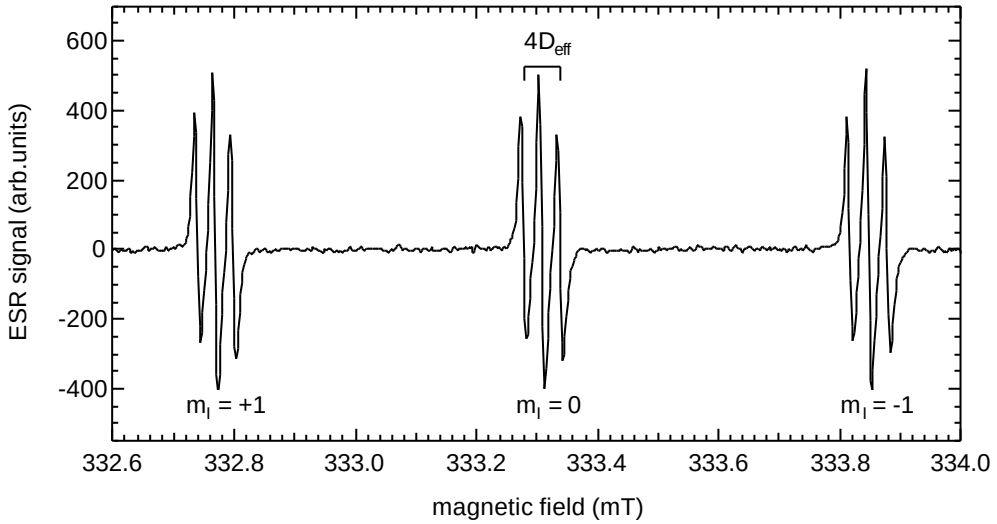

Fig. 5.7: The ESR spectrum of N@C_{70} in MBBA. The splitting of each of these lines is due to the orientation of the symmetry axis of C_{70} with respect to the external magnetic field. D_{eff} is the mean finestructure value describing the orientation of the C_{70} molecules in the liquid crystal. The splitting shows that the molecules are uniquely oriented with respect to the external field.

As shown in Fig. 5.7 for N@C_{70}, the finestructure interaction splits each hyperfine line into three lines: one at the original position, one shifted to lower, and one shifted to higher fields. The value of $D_{eff}/g_e\mu_B$, deduced from the $m_I = 0$ hyperfine line where the splitting is not affected by the second–order hyperfine interaction, is $D_{eff}/g_e\mu_B$ = 14.9 (1) µT. The width of the centre line at 299 K is 6.07 (40) µT, the outer lines being

slightly broader by 20%. The line intensities exhibit the expected ratio of 3:4:3 for the outer, centre, outer line, respectively.

Fig. 5.8 shows the temperature dependence of D_{eff} for $N@C_{70}$ in MBBA. It can be seen that the measurements performed at room temperature are close to the maximum value observed in the supercooled nematic (solid) phase. The transition to the isotropic phase is marked by the disappearance of the splitting. It occurs in the temperature range where the phase transition of pure MBBA is known to take place [**12**]. The $N@C_{70}$ concentration of about 0.1 mM is very low and probably does not alter the phase transition.

As long as size and sign of the order parameter O_{33} are not known, only an lower limit $|D/g_e\mu_B| = 14.9\ (1)\ \mu T$, corresponding to $O_{33} = 1$, can be deduced. A decomposition of D and O_{33} can be done comparing the temperature dependence of the nitrogen hyperfine coupling in MBBA with ENDOR studies of polycrystalline samples [6]. This has been done in ref. [14] yielding $D/g_e\mu_B = 82\ (14)\ \mu T$ and $O_{33} = 0.18\ (3)$.

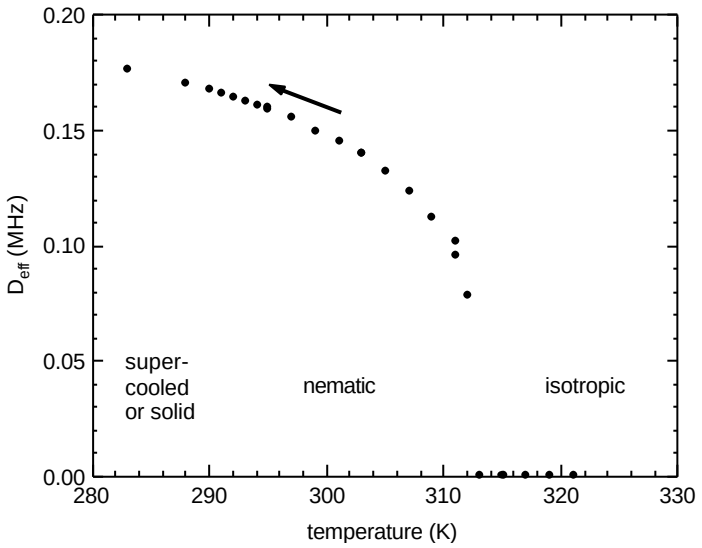

Fig. 5.8: Temperature dependence of the effective finestructure interaction D_{eff} for $N@C_{70}$ in a MBBA liquid crystal. The data were taken in the cooling direction where a supercooled intermediate region occurs at temperatures below about 290 K. In a measurement with increasing temperatures, the line splitting below 290 K could not be determined since the lines were too broad.

C_{60}, other than C_{70} with its elongated shape, has no natural axis for alignment in a liquid crystal. However, as Fig. 5.9 shows, there is also a splitting of the ESR line, and thus an alignment for $N@C_{60}$. The line splitting at 296 K gives $D_{eff}/g_e\mu_B = 3.4\ (2)\ \mu T$, more than a factor of four smaller than the corresponding value for $N@C_{70}$. The widths of the lines (corrected for the modulation broadening) are 3.8 (1) µT with no noticeable difference between the outer lines and the centre line.

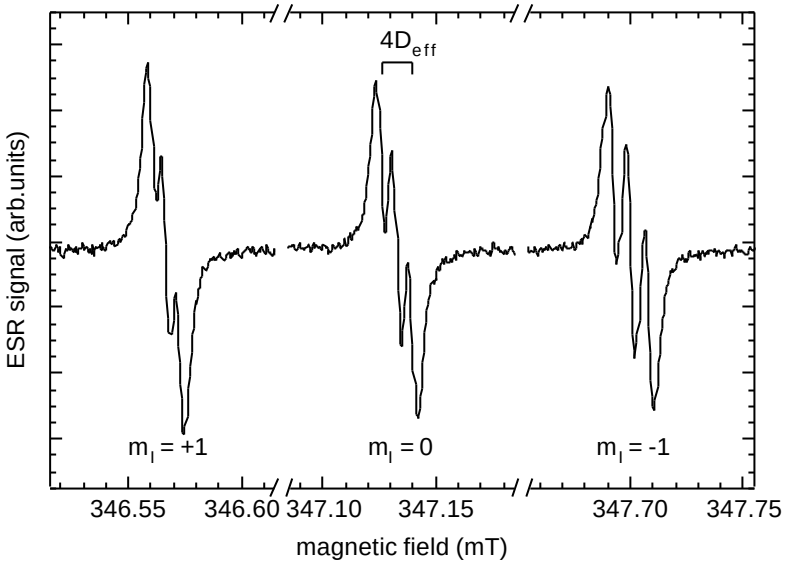

Fig. 5.9: ESR spectrum of N@C_{60} in MBBA liquid crystal at 296 K. Note that the field axis is interrupted between the lines in order to emphasise the splitting. The magnetic quantum number m_I of the nuclear spin I = 1 and the splitting of the outer lines by $4D_{eff}$ (see text) for the m_I = 0 hyperfine line are indicated. The splitting is slightly different for the different m_I multiplets due to a second–order hyperfine splitting.

A break of the spherical symmetry of fullerene molecules has been observed in crystalline C_{60}, where neighbouring C_{60} molecules impose a potential sufficient for ordering at low temperatures. X-ray diffraction measurements [15,14] revealed a non-uniform charge density distribution of C_{60} even at room temperature where the molecules rotate rapidly. This observation implies that the deviation of the charge cloud from uniformity remains fixed in space even if the constituent parts of the fullerene rotate freely. A similar situation is supposed to exist in the presently studied liquid crystal system. Here, we have direct spectroscopic evidence for this deformation at room temperature.

Most other experiments in this context were performed in the low temperature, simple cubic phase of crystalline C_{60}. Raman measurements show a splitting of lines due to crystal field effects [17,18]. The experiment closest to the present one is the EPR measurement on diluted N@C_{60} in polycrystalline C_{60} below the phase transition temperature of 260 K [19]. There, a well resolved powder pattern originating from the finestructure interaction with $D/g_e\mu_B$ = 18.6 µT is observed. This value is approximately five times larger than $D_{eff}/g_e\mu_B = O_{33}\cdot D/g_e\mu_B$ in the present case. Considering that the order parameter O_{33} may be similar for N@C_{60} and N@C_{70} in MBBA, the intrinsic D value, which represents the induced deformation of N@C_{60}, is of similar magnitude in the liquid crystal and in solid state.

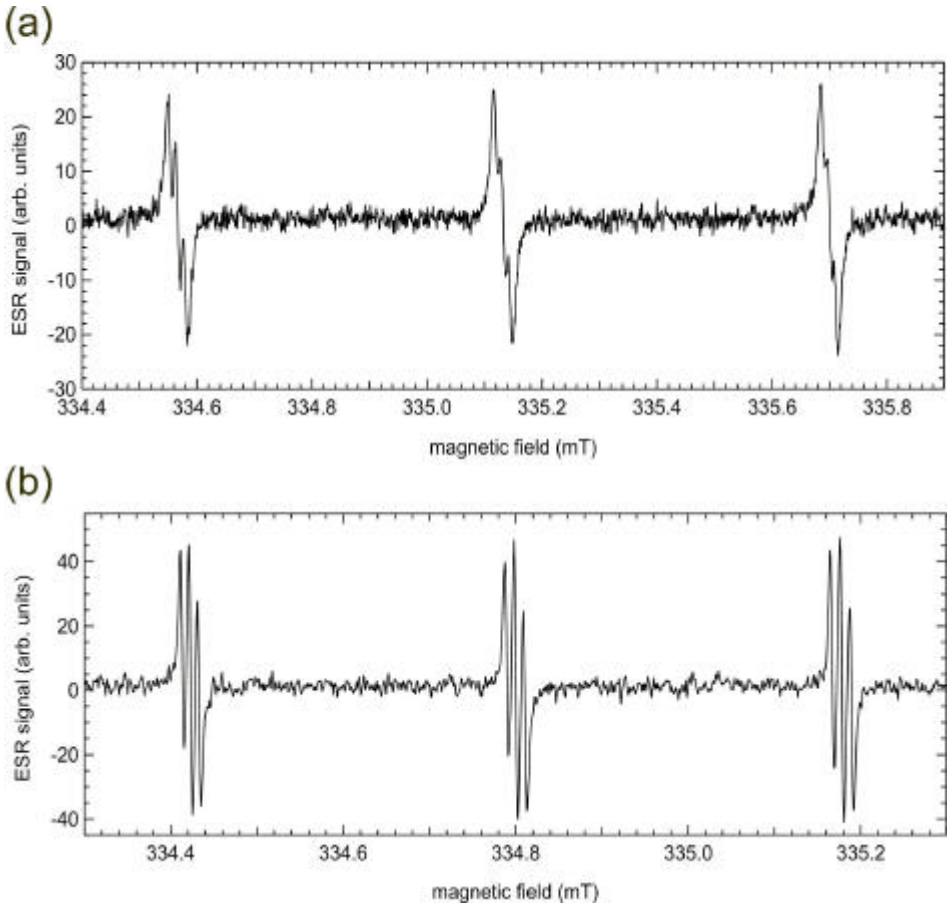

Fig. 5.10: ESR spectra of N@C_{60} in the liquid crystal mixtures ZLI 1695 and ZLI 1289. (a) N@C_{60} in ZLI 1695 has a zero–field splitting D_{eff} of opposite sign compared to MBBA. This is indicated by the field dependence of the line splitting which decreases with increasing field due to second order hyperfine coupling. The splitting in MBBA increases with the field strength. (b) The value of D_{eff} of N@C_{60} in ZLI 1289 is much larger than in MBBA.

N@C_{60} has been dissolved in two other liquid crystal mixtures ZLI 1695 and ZLI 1289 (both obtained from Merck). In Fig. 5.10(a), one can see that for the first one, the induced D is of opposite sign (a negative order parameter has no physical meaning), while D_{eff} of the second in Fig. 5.10(b) is larger than in MBBA (see Tab. 5.1). In this case one cannot distinguish whether the induced zero–field splitting or the order parameter of the liquid crystal changes. Zero–field splitting and linewidth of different endohedral fullerenes are compared in Tab. 5.1.

It is noteworthy that the widths of ESR transitions in the liquid crystal are significantly larger than the linewidth of 0.1 µT as observed in toluene and CS_2 [20]. Two broadening effects may be considered: i) fluctuations of the effective finestructure parameter due to cage deformations induced by collisions with the molecules of the solvent [19] and ii) dipolar broadening due to the nuclear moments of the ^{13}C isotopes on the fullerene cages and the proton moments of the solvent.

Both interactions, finestructure and nuclear dipole, cause variances of the ESR frequencies. The rather small linewidth observed here indicates that some motional narrowing takes place in the liquid crystal, but the narrowing is less complete than in the usual solvents Toluene or CS_2. This is expected, since the mass and shape of the solvent molecules and the viscosity of the solvent material suggest that the motion is slower, i.e. that the correlation time is longer. Of course, this applies also for different liquid crystals. The molecules of the ZLI compound liquid crystals are larger than MBBA and thus, the ESR lines are broader.

Tab. 5.1: Finestructure parameter $D_{eff} = O_{33}D$ and average widths of the lines (see text) from the present experiments for $N@C_{60}$ and $N@C_{70}$ in comparison with the axial parts of the finestructure for solid $N@C_{60}$ [19], the mono–adduct $N@C_{61}(COOC_2H_5)_2$ [7], and the half filled dimer $N@C_{60}-C_{60}$ [8].

	$D_{eff}/g_e\mu_B$ or $D/g_e\mu_B$ (μT)	linewidth (μT)
$N@C_{70}$ in MBBA	82 (14)	6.07 (40)
$N@C_{60}$ in MBBA	3.4 (2)	3.8 (1)
$N@C_{60}$ in ZLI 1695	-6.1[a]	7.5
$N@C_{60}$ in ZLI 1289	7.8	5.4
$N@C_{60}$ in solid, T < 260 K	18.6	
$N@C_{61}(COOC_2H_5)_2$	215	
N@Saturn	460	
$N@C_{60}-C_{60}$	480	

[a] *The sign is defined in this way for convenience. In fact it can be shown, that D is positive in ZLI 1695 and negative in all other cases [14].*

Effects originating from unresolved hyperfine couplings could also contribute to the line width. Taking the natural abundance of 1.11% of the ^{13}C isotope, 49% of C_{60} and 54% of C_{70} have one or more ^{13}C nuclei on the cage. The couplings with nuclear moments are estimated to be in the order of 400 kHz for both cages, using values determined by an analysis of powder ENDOR spectra of $N@C_{60}$ [19]. In a liquid crystal, only values projected on the unique molecular axis are time invariant and have to be considered because of rapid rotation about this axis. The product of this value with the order parameter O_{33} finally leads to an effective hyperfine coupling in the nematic phase. Using the order parameter $O_{33} = 0.18$ deduced for $N@C_{70}$ in MBBA, the coupling is reduced to 72 kHz. Because of a linewidth of 106.4 kHz for $N@C_{60}$ in MBBA, the predicted sub–components could not be resolved.

It has been shown that $N@C_{60}$ and $N@C_{70}$ can be oriented by embedding them into liquid crystals. The degeneracy of the finestructure lines is lifted and the (1/2, -1/2) and the (3/2, 1/2) transitions could be addressed selectively as sufficient in a QCA scheme.

For a proof–of–principle, however, a quantum register consisting of two or three qubits has to be constructed and aligned.

5.3 Towards a two Qubit System

The most simple molecule that can serve as a two qubit system is the fullerene dimer $(C_{60})_2$. It is formed by mechano chemical synthesis, a "soft" method that can be applied after ion implantation of the monomers. Highly enriched material is needed for a "doubly–filled" dimer $(N@C_{60})_2$ and difficult to obtain at present. However, a single nitrogen atom inside is enough to detect the orientation of the molecules, the less elaborate "half–filled" dimer $N@C_{60}–C_{60}$ was used in the following experiments. The synthesis of the half–filled dimer has been done together with Peter Jakeš, TU–Darmstadt.

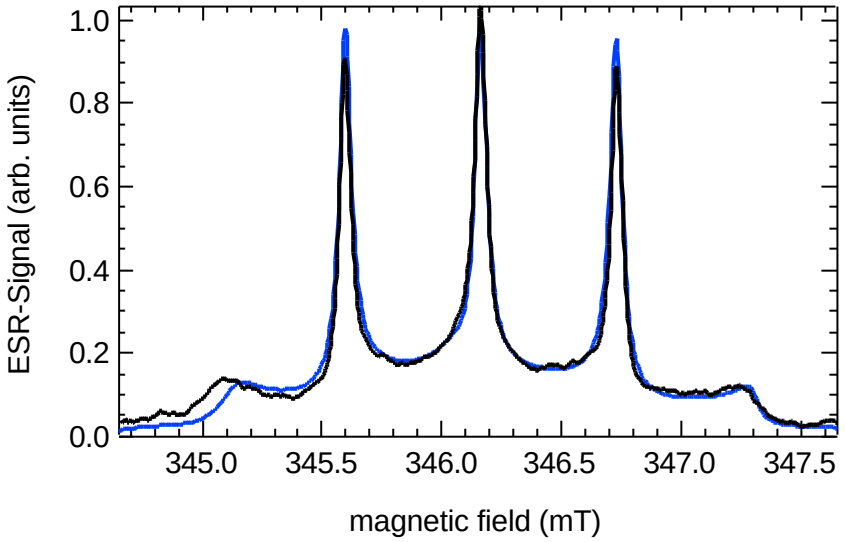

Fig. 5.11: ESR spectrum of a powder sample of half–filled dimers $N@C_{60}–C_{60}$ measured in a cw experiment with 20 µW microwave power and 30 µT modulation amplitude. The material has been synthesised very cautiously, so that no impurities interfere with the signal of the nitrogen spin.

The material used for the dimer synthesis was enriched by a factor of 10 (two steps with HPLC) up to a quality of $\sim 10^{-3}$. About 100 µg of this material were subsequently ball–milled with a mixture of 5mg $AlO_2/CaCl_2$. The dimer yield is ~20%. The dimers were separated from the remaining fullerene molecules by HPLC using a Buckyclutcher column, while the $N@C_{60}/C_{60}$ is collected for recycling. This process was repeated until 90% of the raw material had been processed.

In Fig. 5.11, the ESR spectrum (black line) of a sample prepared from this processed material is shown. As can be seen from the simulation (blue line) with the parameters $D/g_e\mu_B$ = 480 µT and $E/g_e\mu_B$ = 30 µT, the signal of the nitrogen spin is very clean. The synthesis had been done very carefully, so that the impurities seen in the N@Saturn spectrum above or in the $N@C_{60}–C_{60}$ spectrum presented in [8] could be avoided. The

linewidth of the $m_I = 0$ hyperfine line is ~ 60 µT and corresponds to the linewidth measured for the monomers after two steps of enrichment [22].

Another sample from the same material was then dissolved and measured in toluene. Afterwards, the solvent was removed on a vacuum line. The remaining powder was dissolved in a liquid crystal. In MBBA, the spectrum was the same as in solution. Thus, the molecules of the liquid crystal are much too small to align the dimers, which tumble freely as in toluene.

In ZLI 1695 the hyperfine lines became very broad ~ 60 µT, as in the powder sample. Again, the liquid crystal molecules cannot align the dimer. However, they seem to be large enough to stop the dimers from tumbling. Thus, dipolar couplings are not averaged out anymore and the lines get broad.

Only in ZLI 1289, which already showed the largest splitting for $N@C_{60}$, a finestructure splitting could be observed. This is shown in Fig. 5.12.

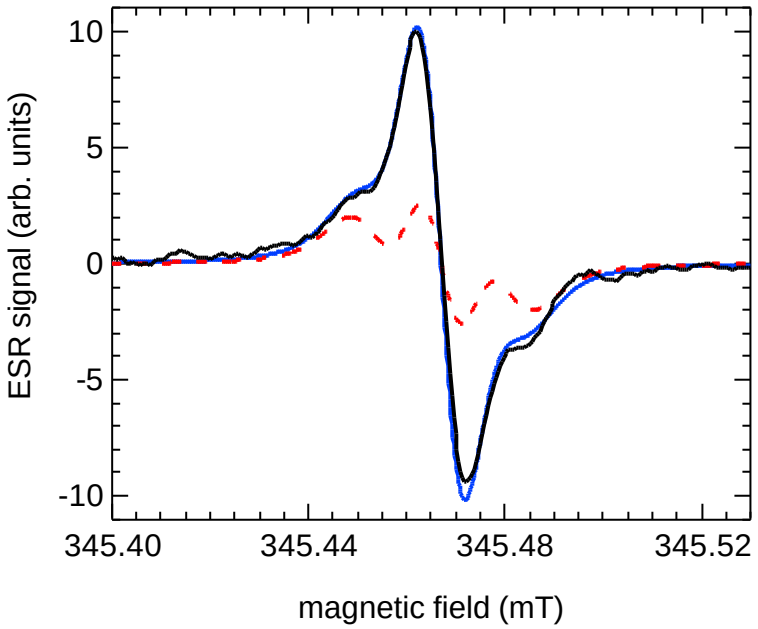

Fig. 5.12: ESR spectrum of the m_I =1 hyperfine line of the half– filled dimer dissolved in the liquid crystal ZLI 1289 (black line). The experiment was carried out at a microwave power of 60 µW with a modulation amplitude of 7 µT. Two signals contribute to the entire spectrum: One part is due to aligned dimers (red dashed line), the other part (a single voigt line) belongs to $N@C_{60}$ monomers. The simulation of the entire spectrum (blue line) yields a line splitting of 13 µT (blue line)

The entire spectrum (black line) seems to be composed of two different signals: One part is due to aligned dimers (red dashed line), the other part belongs to $N@C_{60}$ monomers and shows up as a single voigt line due to modulation broadening. No contribution of $N@C_{60}$ monomers had been found in the powder spectrum of the material (Fig. 5.11). Therefore, the dimers were destroyed by reactions with the liquid crystal and/or during the ultrasonic procedure. The simulation of the spectrum (blue

line) shows that the integrated intensity of the two signals is the same. Thus, half of the dimers have been decomposed while dissolving them in the liquid crystal.

The signal due to the aligned dimers shows a zero–field splitting of $2D_{eff}/g_e\mu_B$ = 13 µT. The linewidth of the centre line is 6.7 µT, while the outer lines are broadened by about 20% just as for N@C_{70} in MBBA. As can be seen in Fig. 5.11, the zero–field splitting of the dimer molecule itself is supposed to be ~ 500 µT. Thus, we can deduce an order parameter of O_{33} ~ 0.013 for the fullerene dimer the liquid crystal ZLI 1289.

In a quantum computing experiment, however, the finestructure transitions have to be addressed selectively. Therefore, the splitting of the lines has to be larger than the linewidth. Besides, the microwave pulses should be kept as short as possible. A frequency width of 188 kHz (corresponding to 6.7 µT linewidth) would require pulse lengths of more than 5 µs. Compared to the phase coherence time, which is also in the µs range, this is much too long, and DiVincenzo's criterion number 3 (see chapter 1) is violated. If a liquid crystal is to be used for the alignment of quantum registers, the order parameter has to be about O_{33} ~ 0.25.

5.4 Conclusions

The N@Saturn molecule presented in this work for the first time can be used to build chains with controlled sequences of (at least) two different endohedral fullerenes. A dimer of this molecule or the "classical" endohedral dimer $(N@C_{60})_2$ oriented in a liquid crystal matrix would provide a short cut to demonstrate the basic ideas of the quantum computing concept presented in chapter 1.

It has been shown that endohedral fullerenes can be oriented by embedding them in a liquid crystal matrix. In principle, this is also possible for dimers, although a liquid crystal with a better order parameter than those tested has to be found. However, a solid state approach, alignment of fullerenes in nano–pores, seems more promising, e.g. chemical reactions with a surface are not expected and low temperature experiments become feasible.

The next step towards a fullerene QCA will be to study the liquid crystal behaviour of doubly filled fullerene dimers. In case of the liquid crystal alignment, the broad powder distribution as calculated by B. Gödde [23] is expected to collapse into separate lines. As long as the linewidth does not exceed 50 µT, the lines are well separated in the solution spectrum. If the linewidth were the same as for the "half–filled" dimer, an order parameter of O_{33} ~ 0.25 would still allow the addressing of the lines.

In this case, the coupling between adjacent spins would be J = 13 MHz. In a powder sample this would correspond to a linewidth of 0.46 mT and selective excitation of resonance lines would be impossible for the dimer. However, if the molecules are aligned in a liquid crystal, the lines will shift rather than broaden because the dipolar interaction is supposed to be identical for all of the aligned dimers.

The endohedral spins can be treated as separate if the coupling is weak compared to the applied magnetic field. They serve as two qubits that can be addressed separately, if their nuclear spins are in a different Zeeman state, like for nitrogen and phosphorous, or if in a different hyperfine state ($m_I = 1/2$ for ^{31}P or ^{15}N). The state preparation can be done with temporal averaging as described by Knill, Chuang and Laflamme in [24].

However, a lot of copies of such a quantum register would be necessary for ensemble read–out. This will be no problem for short fullerene chains, consisting of two, three or four molecules. But, with increasing number of qubits, it will be difficult to produce identical copies that have exactly the same orientation in the magnetic field. Orientation on a surface might then be a more successful approach. In this case, however, single spin read–out techniques have to be available.